

Online Test-time Adaptation for 3D Human Pose Estimation: A Practical Perspective with Estimated 2D Poses

Qiuxia Lin¹ Kerui Gu¹ Linlin Yang^{2,3} Angela Yao¹

¹Department of Computer Science, National University of Singapore

²State Key Laboratory of Media Convergence and Communication, CUC

³School of Information and Communication Engineering, CUC

{qiuxia, keruigu, ayao}@comp.nus.edu.sg

Abstract

Online test-time adaptation for 3D human pose estimation is used for video streams that differ from training data. Ground truth 2D poses are used for adaptation, but only estimated 2D poses are available in practice. This paper addresses adapting models to streaming videos with estimated 2D poses. Comparing adaptations reveals the challenge of limiting estimation errors while preserving accurate pose information. To this end, we propose adaptive aggregation, a two-stage optimization, and local augmentation for handling varying levels of estimated pose error. First, we perform adaptive aggregation across videos to initialize the model state with labeled representative samples. Within each video, we use a two-stage optimization to benefit from 2D fitting while minimizing the impact of erroneous updates. Second, we employ local augmentation, using adjacent confident samples to update the model before adapting to the current non-confident sample. Our method surpasses state-of-the-art by a large margin, advancing adaptation towards more practical settings of using estimated 2D poses.

1. Introduction

Human pose estimation is common in applications where data arrives in video streams. Directly applying pre-trained models can be challenging if the video streams differ from the training data. Online test-time adaptation (OTTA) offers a practical solution because it continuously update the model based on the new data from the testing phase [17, 31, 32]. In 3D pose estimation, a typical strategy is to leverage 2D poses as a weak supervision, assuming that the poses are accurate [3, 24]. Previous works [5, 6] show an idealized proof-of-concept with ground truth poses. Using estimated poses, as the task is intended, however, is more challenging; applied naively, it leads to catastrophic failures where errors even increase (see Table 1 (a)). This work investigates the

underlying reasons and tackles the challenges of adapting 3D pose models to streaming videos with estimated 2D poses.

The conventional setting uses the adapted model from the previous frame as an initial model and then adapts for the current frame based on the current 2D poses. [6, 28, 29] While feasible with ground truth 2D poses, this “single stream” pipeline breaks down with noisy, estimated poses. The breakdown is exacerbated by the limited number of frames/poses used in the update. This presents the challenge of limiting the impact of errors while preserving pose information. Ideally, the adaptation strategy should be adjusted depending on the 2D pose accuracy. In practice, as the accuracy is unknown, we use the 2D estimator confidence as a proxy [4, 11] to partition the keypoints and propose dedicated adaptation solutions for confident and non-confident poses.

First, to limit the impact of estimated 2D pose errors, we propose an alternative “per-video stream” baseline. This baseline re-initializes the model state back to the pre-trained model and performs a separate streaming update on each video. Such an approach eliminates incorrect updates accumulated from previous videos [32]. Yet a full re-initialization wastes the opportunity to learn from the adaptations of the streamed test domain. To concurrently suppress error accumulation while leveraging historical data, we strengthen the “per-video stream” baseline with an adaptive aggregation. The aggregation is performed before the adaptation of each video starts. Specifically, we select representative frames from historical data based on accuracy and diversity. We then leverage 2D poses from non-confident samples and both 2D and 3D poses from confident samples.

For each video, adapting to 2D poses inevitably creates a trade-off: insufficient adaptation loses the opportunity to benefit from the 2D data, while too much can introduce error and over-fitting. To address this, we propose a two-stage optimization for each test sample. In the first stage, we temporarily stop the update based on feature discrepancies. We copy and store the model as the initialization for the next

sample to prevent 2D errors from affecting future samples; in the second stage, the update continues until the projected and estimated 2D poses closely align, providing the 3D prediction for the current sample. Separating the adaptation reduces the impact of error while maintaining fitting benefits.

Secondly, we observe that pose estimation may fail catastrophically in scenes with occlusions, truncations, and rare poses. The failures are sporadic and interspersed throughout video sequences while past samples may be less problematic. In this case, we propose local augmentation to mimic the challenging conditions while leveraging confident adjacent samples. Limiting to only nearby confident samples ensures that the adaptation process is efficient and directly relevant to the failed samples. Summarizing our contributions, we:

- Reveal the key challenge that limits the naive use of estimated 2D poses for 3D human pose adaptation on streaming videos – limiting error propagation while preserving information from estimated 2D poses.
- Propose adaptive aggregation and two-stage optimization to limit the impact of errors while retaining accurate pose information. This involves re-initializing and enhancing the model with representative historical data and a separate adaptation process for each test sample.
- Propose local augmentation to leverage confident samples to improve performance on non-confident ones.
- Achieve up to a 18.0% MPJPE improvement over state-of-the-art, highlighting the benefits of different handling strategies for confident and non-confident poses.

2. Related Work

3D Human Mesh Recovery with 2D Labels. Obtaining accurate 3D labels for in-the-wild data is challenging, so using 2D poses to refine 3D mesh recovery results is a common strategy. The refinement is typically achieved by a projection loss that enforces 2D alignment between the 2D poses and projected 3D mesh [2, 11, 15, 35]. SMPLify [2] incorporates additional constraints to optimize the SMPL parameters for fitting 2D keypoints. EFT [11] instead refines these predictions by fine-tuning the HMR estimation network weights. While effective, these approaches are typically frame-based and do not consider the streaming nature of video data.

Other approaches like DynaBOA [6] and ISO [37] perform streaming adaptation. However, they are not robust because they require 2D ground truth poses. Their performance suffers with estimated poses and this is the setting that we target. Our work, like DynaBOA, leverage guidance by storing samples. However, a key difference is that we use only unlabeled target samples and store a limited number of representatives, which we feel is better aligned with the spirit of OTTA. In contrast, DynaBOA stores labeled training samples from the source domain.

Unsupervised Adaptation on Streaming Data. This work focuses on video – a common form of streaming data where

consecutive frames share a high similarity. It is natural to consider sequential adaptation, which has been used in other tasks such as object tracking [22], semantic segmentation [17, 32], and object recognition [16]. In these tasks, only the streamed video is accessible, so the main challenge is to avoid over-fitting while still learning (unsupervised) from the video stream. Commonly used strategies include feature alignment [16], meta-learning [22], partial fine-tuning [17], and resetting [32]. Adapting 3D HMR in streaming video differs slightly because 2D detected poses are easily accessible and can be used as weak forms of supervision for the adaptation. Different from [5, 6] that uses 2D poses indiscriminately (since they only consider ground truth 2D poses), we target noisy 2D to effectively exploit the beneficial information while mitigating the impact of noisy data.

Learning with Noisy Labels. A straightforward approach is to identify noisy samples and either exclude [7] or down-weight them [18] during model training. Some works consider model output to correct the loss dynamically [1, 25]. Alternatively, noisy labels can be considered by improving model robustness, *e.g.* by augmenting the clean labels [8]. [21] corrects 3D pose predictions generated from noisy 2D labels by cyclically performing motion denoising with the pose estimation. Given the unpredictability of noise and constraints on training time, our method tries to filter out noisy samples while leveraging the similarity between consecutive frame samples to improve the model robustness to noise.

3. OTTA on 3D Human Pose Estimation

3.1. Preliminaries

Framework. We construct a CNN with an iterative regression module as the 3D human pose and shape estimation model \mathcal{M}_ϕ , as per [12]. The model takes an RGB image as input and gives $\{\hat{\theta}, \hat{\beta}, \hat{\mathbf{t}}\}$ as output, where $\hat{\theta} \in \mathbb{R}^{72}$, $\hat{\beta} \in \mathbb{R}^{10}$ are SMPL model [19] pose and shape parameters, and $\hat{\mathbf{t}} \in \mathbb{R}^3$ represents the root joint’s camera-relative translation.

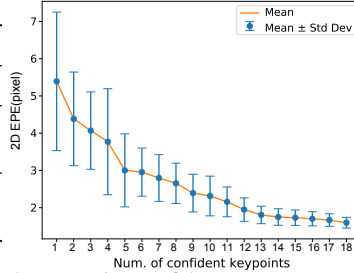
2D weak supervision. The 3D human pose is refined by projection into 2D and comparison with 2D pose labels. Based on the recovered mesh from $\{\hat{\theta}, \hat{\beta}\}$, forward kinematics can be performed to obtain the estimated 3D pose $\hat{\mathbf{p}}_{3d} \in \mathbb{R}^{J \times 3}$ where J is the number of keypoints. The 3D pose $\hat{\mathbf{p}}_{3d}$ is projected into 2D pose $\hat{\mathbf{p}}_{2d} \in \mathbb{R}^{J \times 2}$ based on the camera projection function Π and the camera translation $\hat{\mathbf{t}}$, before comparing with the ground truth \mathbf{p}_{2d} with a projection loss:

$$\mathcal{L}_{2D} = \|\Pi(\hat{\mathbf{p}}_{3d}, \hat{\mathbf{t}}), \mathbf{p}_{2d}\|_2^2. \quad (1)$$

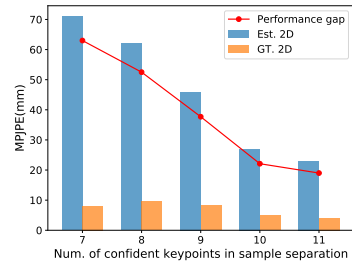
Above, the ground truth pose can also be replaced by an estimated pose $\tilde{\mathbf{p}}_{2d} \in \mathbb{R}^{J \times 2}$ from an off-the-shelf 2D pose estimation framework [3, 24, 34]. Typically, such frameworks also provide a confidence measure $\mathbf{c} \in \mathbb{R}^J$ that roughly represents the prediction accuracy.

Method	2D pose	MPJPE	PA-MPJPE
No adaptation	-	233.3	116.8
Single stream	GT	65.5	40.4
Per-video stream	GT	78.6	46.3
Single stream	Estimated	138.5	79.2
Per-video stream	Estimated	120.4	73.8

(a) Comparison of adaptation settings.



(b) Keypoint confidence vs. pose error.



(c) Estimated vs. GT Performance

Table 1. (a) Adaption of DynBOA [6] on the 3DPW [30] test set using “single stream” vs “per-video stream” pipelines, with ground truth 2D and poses estimated with OpenPose [3]. Adaptation outperforms no adaptation; with ground truth poses, the single stream is better than the per-video stream, but the trend reverses for noisy, estimated poses due to error accumulation. (b) Relationship between the number of confident keypoints and the 2D EPE (pixel) on 3DPW test set. High 2D error samples can be filtered out by keypoint confidence. (c) A significantly larger performance gap (MPJPE [mm]) between using estimated 2D and ground truth 2D labels is observed in samples with fewer confident keypoints. Results are based on the 3DPW test set with “single stream” pipeline.

Problem Formulation. Consider a model \mathcal{M}_{ϕ_0} pre-trained on a labeled 3D human dataset \mathcal{D}_s with ground truth poses $\{\theta, \beta\}$. Online test-time adaptation is performed on the test data $\mathcal{D}_t = \{V_1, V_2, \dots, V_n\}$ where the videos can differ in backgrounds, camera views, etc., in real scenarios. The sequence $V_i = \{x_{i1}, x_{i2}, \dots, x_{im}\}$ denotes the frames in video i , while x_{ij} denotes frame j from video V_i . The test frames arrive sequentially and for each frame x_{ij} , the model is adapted from $\mathcal{M}_{\phi_{i(j-1)}}$ to $\mathcal{M}_{\phi_{ij}}$, with the help of only previous frames $\{x_{i1}, \dots, x_{i(j-1)}, x_{ij}\}$ and their 2D poses. Previous work adopted a “single stream” pipeline that \mathcal{M}_{ϕ} is updated continuously by the incoming frames with 2D ground truth poses, not only within each video but also across videos. However, in practice, 2D ground truth poses for arbitrary videos are unavailable. Our work tackles adaptation with estimated 2D poses in a realistic setting.

3.2. Challenges of using Estimated 2D Poses

What happens when ground truth 2D poses are replaced with estimated ones for adapting the 3D model? The following experiments on the state-of-the-art DynaBOA [6] highlight some key differences that motivate our development.

Table 1(a) shows that using estimated 2D poses in a “single stream” pipeline approximately doubles the errors compared to using ground truth poses. This pipeline, which feeds in videos consecutively, is common practice in OTTA scenarios [6, 27, 29], regardless of differences across the videos. We consider an alternate “per-video stream”¹ baseline, which resets the model to \mathcal{M}_{ϕ_0} when video V_i ends. Such a simple change (per-video stream w/ Est. 2D) significantly improves adaptation results over the “single stream” with estimated 2D poses.

A key difference between ground truth and estimated 2D poses arises in challenging scenarios like occlusions, trun-

¹Our naming convention aligns to the use of established datasets with individual videos; in real-world application streams, natural breaks also occur, e.g. switching cameras on/off, new sessions, new users, etc.

cations, or rare poses. In these cases, pose estimation often fails; it also leads to keypoints with low confidence estimates. Poses with more confident keypoints (we use a confidence threshold of 0.8) generally have lower 2D errors, as shown in Table 1 (b). We consider test poses as confident if they have more than 10 keypoints with confidence estimates above 0.8. Table 1 (c) shows an increasing performance gap of 3D adaptation error between using estimated 2D and ground truth 2D as the number of confident keypoints decreases. It highlights the need to improve these more challenging samples.

4. Methodology

We propose a unified framework to reduce the impact of noisy 2D estimations and improve the 3D adaptation performance on non-confident 2D estimates. First, we introduce an **Adaptive Aggregation** (Sec. 4.1) that changes the streaming pipeline to update the model only with reliable and representative samples. Secondly, we introduce a **Two-Stage Optimization** process (Sec. 4.2) during the adaptation of each sample. Third, to improve performance on non-confident samples, we propose **Local Augmentation** (Sec. 4.3) by leveraging nearby confident samples.

4.1. Adaptive Aggregation

Continuous adaptations over long video streams makes the model more susceptible to inaccurate 2D estimates. To address this, we first base our method on the “per-video stream”, which resets the model each time a new video is encountered. To leverage historical data from other videos, however, we incrementally update the reset model using representative samples selected from past videos.

The simplest way to incorporate past data is through uniform sampling. However, confident and non-confident samples are not uniformly distributed and present different properties. Confident samples have smaller pose errors, but exhibit limited poses and scenes. Conversely non-confident

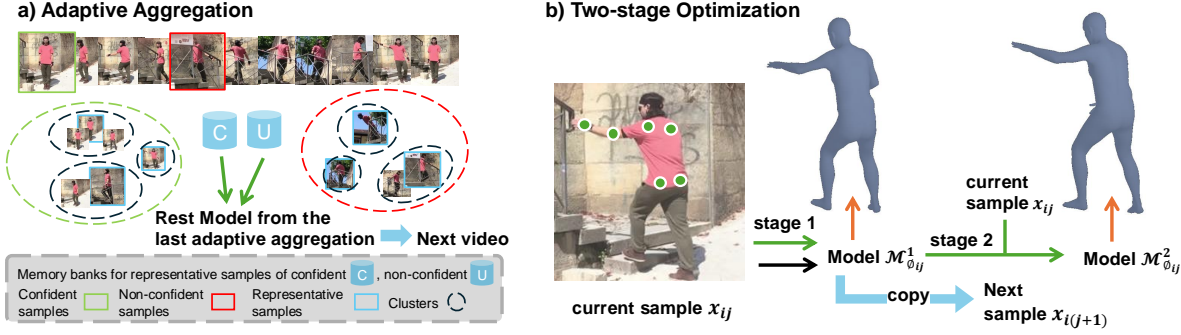


Figure 1. (a) Adaptive Aggregation: Representative samples from both confident and non-confident data are selected using spherical K-means, with memory banks storing these samples for limited retrieval during video transitions. (b) Two-stage Optimization: Each sample undergoes two-stage adaptation to maintain 2D fitting and minimize incorrect updates.

samples have higher pose errors but are drawn from a richer set of poses and scenes (occlusions, truncation). To use both types of samples, we propose three key components in Adaptive Aggregation after resetting the model: 1) Balanced sample selection, 2) Pose clustering, and 3) an Adaptive pseudo-labeling loss.

Balanced sample selection. For the reset model to learn the distribution from both confident and non-confident samples, we split the video data into these two subsets according to the number of confident estimated 2D keypoints and select a balanced number of samples from each subset. To further distinguish the selection, we assign a sampling weight for each sample based on the average 2D confidence:

$$\mathcal{W} = \sum_{j=1}^J c_j / J. \quad (2)$$

Pose clustering. Within both the confident and non-confident subsets, the high sampling weights are associated with a limited set of poses. As such, we apply Spherical K-means clustering [9] on the 3D poses in each subset. As each sample is assigned a sampling weight (See Eq. 2), we order the samples within each cluster by weight and select a specific number based on the ratio of the cluster size to the intended total sampling size $\mathcal{C}_i N_v / \sum_{i=1}^{N_C} \mathcal{C}_i$, where \mathcal{C}_i represents the size of cluster i , N_C is the number of clusters and N_v is the required total sampling number in each video. The selected N_v samples are stored within the subset \mathcal{D}_m for use in the adaptive aggregation.

Adaptive pseudo-labeling loss. Since there is no ground truth label and the adapted results may be supervised by incorrect 2D poses, we adopt an adaptive pseudo-labeling loss. Specifically, we apply a strong pseudo-labeling loss based on 2D and 3D labels for the confident samples and a weak pseudo-labeling loss with only 2D labels for the

non-confident samples:

$$\begin{aligned} \mathcal{L}_{adapt} = & \|T_w^{-1}(\hat{\mathbf{p}}'_{2d}), \tilde{\mathbf{p}}_{2d}\|_2^2 + \mathbb{1} \lambda_2 \|T_w^{-1}(\hat{\mathbf{p}}'_{3d}), \hat{\mathbf{p}}_{3d}\|_2^2 \\ & + \lambda_1 (E_{\hat{\theta}}(\hat{\theta}) + E_{\hat{\beta}}(\hat{\beta})). \end{aligned} \quad (3)$$

Above, the first and the second loss term enforces 2D and 3D consistency, respectively; the third term is a prior applied to the shape and pose parameters, similar to [5, 13]. The indicator $\mathbb{1}$ indicates the additional strong pseudo-labeling term for the confident samples. In both terms, we encourage consistency between the predicted $\hat{\mathbf{p}}_{3d}$, estimated $\tilde{\mathbf{p}}_{2d}$ of the original image and transformed-back predictions $\hat{\mathbf{p}}'_{3d}$, $\tilde{\mathbf{p}}'_{2d}$ of the augmented image. T_w represents the geometric transformation including rotation, scaling, translation, that we apply on the original images to get corresponding augmented ones. T_w^{-1} denotes the reversed transformation. Symbols with a prime superscript denote the predictions on the augmented images, to distinguish them from predictions on the original image. For non-confident samples, we apply weak pseudo-labelling loss for only utilizing 2D information.

We perform adaptive aggregation when the video changes, selecting N_v samples from \mathcal{D}_m to train the reset model using adaptive pseudo-labeling loss. To prevent earlier samples added to \mathcal{D}_m from being selected more frequently than others, we apply a selection probability on each sample in \mathcal{D}_m , which is inversely proportional to the number of times it has been previously chosen. Instead of following ‘‘single stream’’ to update model across videos, which transits the incorrect updates from the previous video to the next video, we use adapted results that are representative to incrementally update the model across videos.

4.2. Two-stage Optimization

Off-the-shelf 2D pose estimators can often provide more accurate 2D estimates than those projected from 3D human pose models, especially when there is a domain gap [20]. This information can be valuable for refining 3D poses. How-

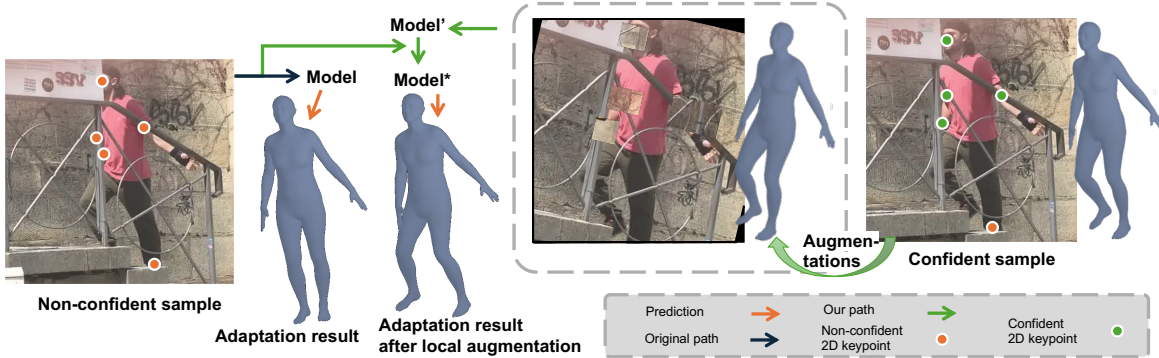


Figure 2. Local augmentation. We augment the temporally adjacent confident samples to simulate the hard features in non-confident samples. The transformed predictions are used to guide the model before adapting to the non-confident sample. Specifically, we first adapt the model using augmented confident samples to obtain Model’. Then, Model’ is further adapted with non-confident samples to obtain the final Model*, which is used for prediction.

ever, errors in estimated 2D poses are inevitable. Adapting the model using these wrong 2D poses can lead to harmful updates, specifically causing low generalization ability to subsequent samples. To address this, we propose a two-stage optimization strategy to enhance the fitting only on the current sample and mitigate the negative influence on the following samples simultaneously.

Given the estimated 2D poses, we first update the model parameters based on the 2D projections of the estimated 3D pose, along with the pose and shape priors.

$$\mathcal{L}_{proj} = \|\Pi(\hat{\mathbf{p}}_{3d}, \hat{\mathbf{t}}), \tilde{\mathbf{p}}_{2d}\|_2^2 + \lambda_1(E_{\hat{\theta}}(\hat{\theta}) + E_{\hat{\beta}}(\hat{\beta})) \quad (4)$$

We aim for the projected 2D poses (from the estimated 3D poses) to align with the estimated 2D poses. After several alignments, due to the potential errors in the estimated 2D poses, the model may start to fail on subsequent samples. As such, we consider a first stage with early stopping [23] when the feature changes stabilize [6]. We measure the cosine similarity between features in a specific layer before and after each iteration based on Eq. 4 with current sample and stop the optimization when the similarity falls below a certain threshold. As illustrated in Fig. 1(b), as the first stage finishes for the input frame x_{ij} , we have the adapted model $\mathcal{M}_{\phi_{ij}}^1$ and pass it to the next sample $x_{i(j+1)}$. To achieve better aligned 2D predictions, we then continue updating the model to $\mathcal{M}_{\phi_{ij}}^2$ until the 2D fitting loss is minimized to the required value for better-aligned 2D predictions. The final 3D adaptation results of x_{ij} is obtained by $\mathcal{M}_{\phi_{ij}}^2$ which will not be utilized in further samples.

4.3. Local Augmentation

For the case where the 2D estimator fails, we designed a local augmentation strategy to leverage confident samples to assist the model prediction on the non-confident samples. The rationale is that the non-confident samples tend to appear unpredictably, often during brief occlusions or when the

human moves out of the camera’s view, while surrounding samples remain unaffected by these challenges, which results in sporadic distribution of non-confident samples.

How can we leverage the previous confident sample with relatively accurate 2D and 3D labels to help the prediction of the current non-confident sample? We observe that the non-confident samples often feature occlusions and truncations, so we apply strong augmentations on previous confident samples to improve model robustness. We provide an illustration in Fig. 2. Strong augmentations, denoted by T_s , includes geometry and texture augmentation, which are rotation, scaling, translation, color normalization, image truncation, and keypoint occlusion. Considering the pose similarity, we only augment the confident sample within a short temporal window before the non-confident sample.

Preliminary experiments show that a window of five frames is appropriate (See Supp.). If a specific keypoint is confident in the former but non-confident in the latter, we will occlude it in the former to simulate the challenges in the latter.

Suppose the model 3D prediction on the original unaugmented confident sample is $\hat{\mathbf{p}}_{3d}$ and the estimated 2D is $\tilde{\mathbf{p}}_{2d}$, the training can thus be supervised by enforcing the consistency between the original predictions and transform-backed predictions $T_s^{-1}(\hat{\mathbf{p}}'_{2d})$, $T_s^{-1}(\hat{\mathbf{p}}'_{3d})$ on the augmented image.

$$\mathcal{L}_{aug} = \|T_s^{-1}(\hat{\mathbf{p}}'_{2d}), \tilde{\mathbf{p}}_{2d}\|_2^2 + \lambda_2\|T_s^{-1}(\hat{\mathbf{p}}'_{3d}), \hat{\mathbf{p}}_{3d}\|_2^2. \quad (5)$$

4.4. Method Overview

Mean-teacher training. We incorporate mean-teacher training [26] as it is widely used in unsupervised learning [6, 14, 36]. It can enhance stability and mitigate the impact of unreliable test data. It involves maintaining both a student and a teacher model. The student model is updated using designed losses, while the teacher model is updated

2D Pose Estimator	Method	<i>Human3.6M</i> \rightarrow <i>3DPW</i>		<i>Human3.6M</i> \rightarrow <i>3DHP</i>	
		MPJPE	PA-MPJPE	MPJPE	PA-MPJPE
OpenPose [3]	DynaBOA	138.5	79.2	132.3	86.4
	CycleAdapt*	123.6	70.5	130.1	85.2
	Ours	101.3	64.5	122.4	82.6
HRNet [24]	DynaBOA	108.0	63.9	130.3	86.8
	CycleAdapt*	102.8	61.2	122.8	83.5
	Ours	95.3	60.6	120.1	80.7
VitPose [34]	DynaBOA	91.8	56.6	118.7	77.7
	CycleAdapt*	90.5	55.8	115.3	75.6
	Ours	87.2	53.5	112.1	73.2
Ground Truth	DynaBOA	65.5	40.4	101.5	66.1
	CycleAdapt*	67.1	44.3	102.1	67.5
	Ours	64.9	40.6	100.8	65.4

Table 2. Robustness to different estimated 2D [3, 24, 34]. Our method demonstrates robustness across 2D inputs of varying accuracy. *Modified CycleAdapt source code to accommodate the online setting.

by temporal weight ensembling of the student model. The reported results come from the student model.

Overall pipeline. Given several test videos $\mathcal{D}_t = \{V_1, \dots, V_n\}$, we adapt the model on them sequentially. For each arriving sample x_{ij} in video i , we apply specific strategies based on its confidence. Confident sample is directly adapted with two-stage optimization (Eq. 4) from model state $\mathcal{M}_{\phi_{i(j-1)}}$ to obtain $\mathcal{M}_{\phi_{ij}}^2$ for inference and $\mathcal{M}_{\phi_{ij}}^1$ for the next sample $x_{i(j+1)}$. If the current sample is non-confident, we use previously confident samples within the temporal window to update the model with local augmentation (Eq. 5) followed by the two-stage optimization. Once adaptation for video i is complete, representative samples are taken through balanced selection and clustering, and stored in \mathcal{D}_m . Prior to processing the next video $i + 1$, the model is first reversed to the initial state of video i , *i.e.*, \mathcal{M}_{ϕ_i} . We then enhance it with adaptive aggregation (Eq. 3) through weighted sampling from \mathcal{D}_m to achieve initial state $\mathcal{M}_{\phi_{i+1}}$ for video $i + 1$. The overall illustration and algorithm can be found in Supplementary Materials.

5. Experiments

5.1. Setup, Datasets & Evaluation

Setup: We use various 2D estimators which provide 2D poses and keypoint confidences: OpenPose [3], HRNet [24], VitPose [34]. The backbone is HMR network [12]. Our method is implemented with Pytorch and trained using Adam optimizer with a momentum of 0.5 and an initial learning rate of 3×10^{-6} . The images are resized to 224×224 . The hyperparameters λ_1, λ_2 are set as $1e-4$ and 10. The seed is 22. The cluster number $N_c = 15$ and the required total sampling number $N_v = 160$ in each video. During adaptive aggregation, we will use Adam optimizer with a momentum of 0.7 and a learning rate of 3×10^{-5} . The batch size

Method	<i>Human3.6M</i> \rightarrow <i>3DPW</i>		<i>Human3.6M</i> \rightarrow <i>3DHP</i>	
	MPJPE	PA-MPJPE	MPJPE	PA-MPJPE
No adaptation	233.3	116.8	218.4	118.4
DynaBOA [6]	138.5	79.2	132.3	86.4
CycleAdapt* [21]	123.6	70.5	130.1	85.2
CycleAdapt ² [21]	90.3	55.2	-	-
ISO [37]	-	70.8	-	-
SMPLify [2]	190.3	97.5	174.8	105.3
EFT [11]	143.6	83.2	152.3	92.1
Ours	101.3	64.5	122.4	82.6

Table 3. For online TTA with estimated 2D poses from OpenPose [3], our method performs best. *Modified CycleAdapt source code to accommodate the online setting.

is 8 in adaptive aggregation and 1 in local augmentation and two-stage optimization. We compare with state-of-the-art test-time adaptation methods (DynaBOA [6], ISO [37], DAPA [33], CycleAdapt [21]) and optimization-based methods (SMPLify [2] and EFT [11]). Note that CycleAdapt is designed for (offline) test-time adaptation; they do not release source code for the online setting, and we modify their code to support it.

Datasets: **Human3.6M** [10] comprises 3.6 million indoor human pose samples with static backgrounds with ground truth 2D and 3D poses. Following protocol 1, we pre-train our model using samples from subjects 1, 5, 6, 7, and 8. **3DPW** [30] is a challenging in-the-wild human pose dataset with extensive occlusions, varied lighting conditions, and truncations. We utilize only its test data, which consists of 24 videos with 35,515 samples. **MPI-INF-3DHP (3DHP)** [20] is another benchmark from which we use the test set to perform model adaptation. The test set contains 6 videos with 2,929 samples across diverse backgrounds including

²Reported from [21]’s Supplementary Table B(a); results not reproducible from provided code.

Method	All	Conf.	Non-conf.
Per-video stream	120.4	117.8	160.5
+adaptive agg.	105.2	103.6	124.7
+local aug.	107.5	106.8	130.5
+two-stage	106.1	104.3	133.8

(a) Component-wise Ablations of MPJPE (mm)

Method	weak pl	strong pl	adaptive pl
Uniform sampling	114.5	116.2	114.3
Weight-based sampling	111.6	115.2	111.5
+Balanced selection	109.5	114.3	107.6
+Pose Clustering	107.7	108.2	105.2

(b) Adaptive Aggregation Ablation

Table 4. (a) Ablation study on the 3DPW test set with MPJPE (mm). Adaptive aggregation (+adaptive agg.) excelled overall. Local augmentation (+local aug.) is better for non-confident samples, while two-stage optimization benefits confident samples more. (b) The adaptive aggregation increases sample diversity and quality.

green screen, in-studio, and in-the-wild settings. The poses are generally more complex than those in 3DPW.

Evaluation: The Human3.6M dataset is used as training data for model pre-training with available annotations. The test set of 3DPW and 3DHP are used as unlabeled test data for model adaptation, thus we can build two test-time adaptation tasks $Human3.6M \rightarrow 3DPW$ and $Human3.6M \rightarrow 3DHP$ to evaluate the proposed method. The applied evaluation metrics are the Mean Per Joint Position Error (MPJPE) between the ground truth and the predicted 3D pose, and Procrustes Aligned MPJPE (PA-MPJPE) with additional 3D alignment. Both are reported in millimeters.

5.2. Results of Online Test-Time Adaptation

Results on 3DPW & 3DHP. Table 3 compares our method with state-of-the-art on two online test-time adaptation tasks. With estimated 2D data, the optimization-based methods [2, 11] perform poorly. Although slightly better, test-time adaptation methods [6, 21, 37] also struggle. These results highlight the challenge of using estimated 2D poses to adapt 3D models. Our method performs best by effectively utilizing estimated 2D data to extract valuable information from the test data.

Robustness to Different 2D Pose Estimators. Table 2 compares our method with DynaBOA and CycleAdapt using different 2D pose estimators [3, 24, 34], with differing levels of accuracy. Our method significantly outperforms DynaBOA on the 3DPW and 3DHP datasets. CycleAdapt improves upon DynaBOA, which targets estimated 2D poses, by reducing noisy 2D poses through motion denoising. However, it still struggles in the online setting due to limited sample optimization with noisy 2D poses. This leads to overfitting during the cyclic update between modules. We propose more refined strategies to handle such extreme cases with noisy labels. The result verifies the ability of our method to improve 3D prediction even when the weak supervising labels (the 2D poses) has errors. As 2D accuracy improves, our method outperforms comparisons and stays competitive with ground truth 2D, showing its robustness.

5.3. Ablation Studies

Table 4 (a) shows that adaptive aggregation, local augmentation, and two-stage optimization all bring improvements.

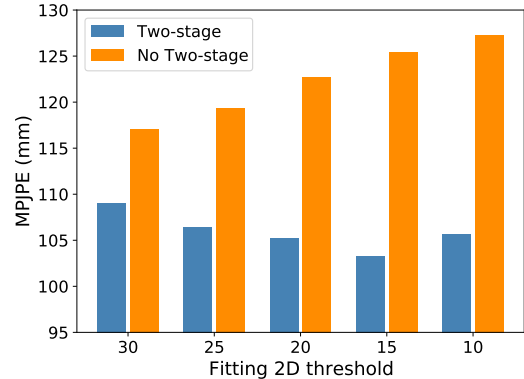
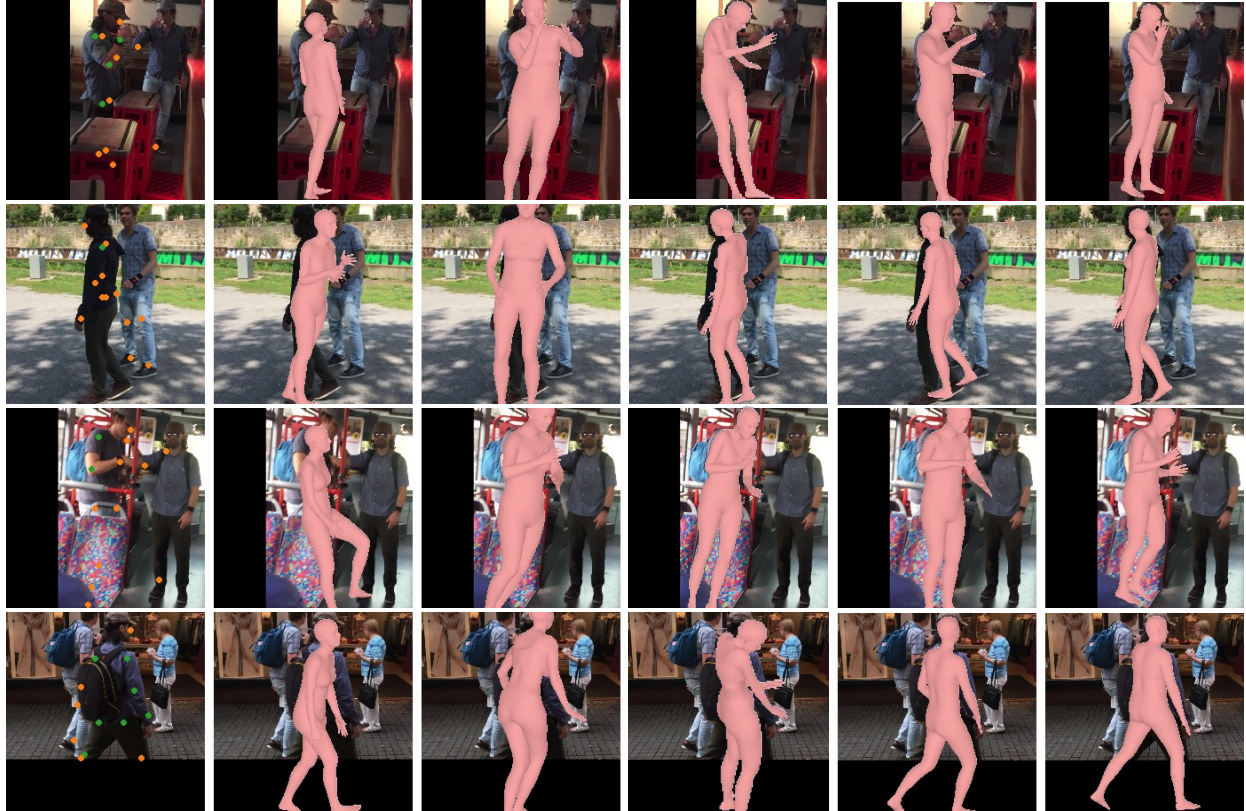


Figure 3. The two-stage optimization benefits from 2D projection while minimizing introduced errors.

Sample selection in adaptive aggregation. Intuitively, the samples used should have low error and be representative of the current video. We find low-error samples by selecting those with high sampling weight; however, exclusively relying on sampling weight will limit pose diversity. Therefore, we separate samples into confident and non-confident subsets and adopt a balanced selection. To maintain pose distribution, we add pose clustering finally. As shown in Table 4 (b), uniform sampling performs worse than weight-based sampling, but the best results are obtained by combining balanced selection and pose clustering.

Other components of adaptive aggregation. To leverage the information based on sample difficulty, we used weak and strong pseudo-labeling adaptively (see Eq. 3). Table 4 (b) shows that using either only weak or only strong pseudo-labeling does not yield better results compared to a strategy where confident samples are subjected to strong pseudo-labeling and non-confident samples to weak pseudo-labeling.

Balance 2D projection and minimizing incorrect updates. In our two-stage optimization, the second stage is stopped based on a 2D projection threshold, as defined in Eq. 1. Fig. 3 shows that, in the two-stage setting, reducing the 2D projection threshold (from 30 to 15) to emphasize the projection guidance leads to improved results, whereas an overly strict threshold of 10 leads to the model incorporating excessive noise. However, without the two-stage optimization, wrongly estimated 2D poses leads to overall impaired per-



(a) Estimated 2D over Image (b) EFT (c) DynaBOA (d) CycleAdapt* (e) Ours (f) Ground Truth

Figure 4. Qualitative results on a 3DPW test sample comparing our method with EFT [11], DynaBOA [6] and CycleAdapt* [21]. We present the estimated 2D results (a) with confident keypoints colored green and non-confident keypoints colored orange. Our method shows better results in challenging cases involving truncation and complex backgrounds. *Modified CycleAdapt source code to accommodate the online setting.

formance. Our two-stage optimization effectively prevents this by maintaining 2D projection benefits and reducing the impact of errors through separation after the first stage.

5.4. Qualitative Results

Fig. 4 visualizes the results of our method compared to others on challenging samples with low-confidence 2D inputs. Our approach demonstrates superior performance by producing more accurate 3D human mesh reconstructions, even in cases with insufficient illumination or truncation. This highlights the robustness of our method in handling difficult scenarios where other methods often fail to provide reliable predictions.

6. Conclusion and Limitations

Adapting the 3D pose model to unseen streaming data with estimated 2D poses is a challenging and practical task. To better solve this problem, we identify the challenge of limiting estimation errors while preserving pose information when using estimated 2D poses. Based on that, we propose

adaptive aggregation, a two-stage optimization, and local augmentation for handling varying levels of estimated pose error. First, we propose adaptive aggregation to re-initialize the 3D model and leverage useful information from the historical data. The influence of wrong updates in each sample adaptation is further minimized through a two-stage optimization. For the non-confident 2D labels that can hardly refine their 3D predictions, we propose local augmentation, which performs augmentation on adjacent confident samples to help the adaptation of the current non-confident sample. Extensive experiments demonstrate the effectiveness of each component and its significant improvement over state-of-the-art methods over two large-scale benchmarks.

However, our method still depends on the quality of the estimated 2D poses. A better solution would be to enhance the 2D data quality during model adaptation as well. Additionally, we use temporally adjacent samples to assist non-confident samples; this strategy could be improved by incorporating richer temporal information from multiple adjacent samples. Addressing these limitations will be future work.

References

- [1] Eric Arazo, Diego Ortego, Paul Albert, Noel O’Connor, and Kevin McGuinness. Unsupervised label noise modeling and loss correction. In *ICML*, pages 312–321. PMLR, 2019. 2
- [2] Federica Bogo, Angjoo Kanazawa, Christoph Lassner, Peter Gehler, Javier Romero, and Michael J Black. Keep it smpl: Automatic estimation of 3d human pose and shape from a single image. In *ECCV*, pages 561–578. Springer, 2016. 2, 6, 7
- [3] Zhe Cao, Tomas Simon, Shih-En Wei, and Yaser Sheikh. Realtime multi-person 2d pose estimation using part affinity fields. In *CVPR*, pages 7291–7299, 2017. 1, 2, 3, 6, 7
- [4] Kerui Gu, Rongyu Chen, Xuanlong Yu, and Angela Yao. On the calibration of human pose estimation. In *ICML*, 2024. 1
- [5] Shanyan Guan, Jingwei Xu, Yunbo Wang, Bingbing Ni, and Xiaokang Yang. Bilevel online adaptation for out-of-domain human mesh reconstruction. In *CVPR*, pages 10472–10481, 2021. 1, 2, 4
- [6] Shanyan Guan, Jingwei Xu, Michelle Zhang He, Yunbo Wang, Bingbing Ni, and Xiaokang Yang. Out-of-domain human mesh reconstruction via dynamic bilevel online adaptation. *TPAMI*, 45(4):5070–5086, 2022. 1, 2, 3, 5, 6, 7, 8
- [7] Bo Han, Quanming Yao, Xingrui Yu, Gang Niu, Miao Xu, Weihua Hu, Ivor Tsang, and Masashi Sugiyama. Co-teaching: Robust training of deep neural networks with extremely noisy labels. *NeurIPS*, 31, 2018. 2
- [8] Trung-Hieu Hoang, Mona Zehni, Huy Phan, Duc Minh Vo, and Minh N Do. Improving the robustness of 3d human pose estimation: A benchmark and learning from noisy input. In *CVPR*, pages 113–123, 2024. 2
- [9] Kurt Hornik, Ingo Feinerer, Martin Kober, and Christian Buchta. Spherical k-means clustering. *SS*, 50:1–22, 2012. 4
- [10] Catalin Ionescu, Dragos Papava, Vlad Olaru, and Cristian Sminchisescu. Human3.6m: Large scale datasets and predictive methods for 3d human sensing in natural environments. *TPAMI*, 36(7):1325–1339, 2013. 6
- [11] Hanbyul Joo, Natalia Neverova, and Andrea Vedaldi. Exemplar fine-tuning for 3d human model fitting towards in-the-wild 3d human pose estimation. In *3DV*, pages 42–52. IEEE, 2021. 1, 2, 6, 7, 8
- [12] Angjoo Kanazawa, Michael J Black, David W Jacobs, and Jitendra Malik. End-to-end recovery of human shape and pose. In *CVPR*, pages 7122–7131, 2018. 2, 6
- [13] Nikos Kolotouros, Georgios Pavlakos, Michael J Black, and Kostas Daniilidis. Learning to reconstruct 3d human pose and shape via model-fitting in the loop. In *ICCV*, 2019. 4
- [14] Chen Li and Gim Hee Lee. From synthetic to real: Unsupervised domain adaptation for animal pose estimation. In *CVPR*, 2021. 5
- [15] Zhihao Li, Jianzhuang Liu, Zhensong Zhang, Songcen Xu, and Youliang Yan. Cliff: Carrying location information in full frames into human pose and shape estimation. In *ECCV*, pages 590–606. Springer, 2022. 2
- [16] Wei Lin, Muhammad Jehanzeb Mirza, Mateusz Kozinski, Horst Possegger, Hilde Kuehne, and Horst Bischof. Video test-time adaptation for action recognition. In *CVPR*, pages 22952–22961, 2023. 2
- [17] Jiaming Liu, Senqiao Yang, Peidong Jia, Ming Lu, Yandong Guo, Wei Xue, and Shanghang Zhang. Vida: Homeostatic visual domain adapter for continual test time adaptation. *ICLR*, 2024. 1, 2
- [18] Tongliang Liu and Dacheng Tao. Classification with noisy labels by importance reweighting. *TPAMI*, 38(3):447–461, 2015. 2
- [19] Matthew Loper, Naureen Mahmood, Javier Romero, Gerard Pons-Moll, and Michael J Black. Smpl: A skinned multi-person linear model. In *ACM TOG*, pages 851–866. 2023. 2
- [20] Dushyant Mehta, Helge Rhodin, Dan Casas, Pascal Fua, Oleksandr Sotnychenko, Weipeng Xu, and Christian Theobalt. Monocular 3d human pose estimation in the wild using improved cnn supervision. In *3DV*, pages 506–516. IEEE, 2017. 4, 6
- [21] Hyeongjin Nam, Daniel Sungho Jung, Yeonguk Oh, and Kyoung Mu Lee. Cyclic test-time adaptation on monocular video for 3d human mesh reconstruction. In *ICCV*, pages 14829–14839, 2023. 2, 6, 7, 8
- [22] Eunbyung Park and Alexander C Berg. Meta-tracker: Fast and robust online adaptation for visual object trackers. In *ECCV*, pages 569–585, 2018. 2
- [23] Lutz Prechelt. Early stopping-but when? In *Neural Networks: Tricks of the trade*, pages 55–69. Springer, 2002. 5
- [24] Ke Sun, Bin Xiao, Dong Liu, and Jingdong Wang. Deep high-resolution representation learning for human pose estimation. In *CVPR*, 2019. 1, 2, 6, 7
- [25] Daiki Tanaka, Daiki Ikami, Toshihiko Yamasaki, and Kiyoharu Aizawa. Joint optimization framework for learning with noisy labels. In *CVPR*, pages 5552–5560, 2018. 2
- [26] Antti Tarvainen and Harri Valpola. Mean teachers are better role models: Weight-averaged consistency targets improve semi-supervised deep learning results. *NeurIPS*, 30, 2017. 5
- [27] Alessio Tonioni, Oscar Rahnama, Thomas Joy, Luigi Di Stefano, Thalaisyasingam Ajanthan, and Philip HS Torr. Learning to adapt for stereo. In *CVPR*, pages 9661–9670, 2019. 3
- [28] Alessio Tonioni, Fabio Tosi, Matteo Poggi, Stefano Mattocchia, and Luigi Di Stefano. Real-time self-adaptive deep stereo. In *CVPR*, pages 195–204, 2019. 1
- [29] Riccardo Volpi, Pau De Jorge, Diane Larlus, and Gabriela Csurka. On the road to online adaptation for semantic image segmentation. In *CVPR*, pages 19184–19195, 2022. 1, 3
- [30] Timo Von Marcard, Roberto Henschel, Michael J Black, Bodo Rosenhahn, and Gerard Pons-Moll. Recovering accurate 3d human pose in the wild using imus and a moving camera. In *ECCV*, 2018. 3, 6
- [31] Dequan Wang, Evan Shelhamer, Shaoteng Liu, Bruno Olshausen, and Trevor Darrell. Tent: Fully test-time adaptation by entropy minimization. *arXiv preprint arXiv:2006.10726*, 2020. 1
- [32] Qin Wang, Olga Fink, Luc Van Gool, and Dengxin Dai. Continual test-time domain adaptation. In *CVPR*, pages 7201–7211, 2022. 1, 2
- [33] Zhenzhen Weng, Kuan-Chieh Wang, Angjoo Kanazawa, and Serena Yeung. Domain adaptive 3d pose augmentation for in-the-wild human mesh recovery. In *3DV*, pages 261–270. IEEE, 2022. 6

- [34] Yufei Xu, Jing Zhang, Qiming Zhang, and Dacheng Tao. ViTPose: Simple vision transformer baselines for human pose estimation. In *NeurIPS*, 2022. [2](#), [6](#), [7](#)
- [35] Fengyuan Yang, Kerui Gu, and Angela Yao. Kitro: Refining human mesh by 2d clues and kinematic-tree rotation. In *CVPR*, 2024. [2](#)
- [36] Longhui Yuan, Binhui Xie, and Shuang Li. Robust test-time adaptation in dynamic scenarios. In *CVPR*, pages 15922–15932, 2023. [5](#)
- [37] Jianfeng Zhang, Xuecheng Nie, and Jiashi Feng. Inference stage optimization for cross-scenario 3d human pose estimation. *NeurIPS*, 33:2408–2419, 2020. [2](#), [6](#), [7](#)